Electronic Supplementary Material

Field-effect at electrical contacts to two-dimensional materials

Yao Guo[1] (✉), Yan Sun[1], Alvin Tang[2], Ching-Hua Wang[2], Yanqing Zhao[1], Mengmeng Bai[1], Shuting Xu[1], Zheqi Xu[1], Tao Tang[3], Sheng Wang[4], Chenguang Qiu[4], Kang Xu[5], Xubiao Peng[1], Junfeng Han[1], Eric Pop[2], and Yang Chai[5] (✉)

[1] *School of Physics, Beijing Institute of Technology, Beijing 100081, China*
[2] *Department of Electrical Engineering and Stanford SystemX Alliance, Stanford University, Stanford, CA 94305, USA*
[3] *Advanced Manufacturing EDA Co., Ltd., Shanghai 201204, China*
[4] *Key Laboratory for the Physics and Chemistry of Nanodevices, Department of Electronics, Peking University, Beijing 100871, China*
[5] *Department of Applied Physics, The Hong Kong Polytechnic University, Hong Kong, China*

Supporting information to https://doi.org/10.1007/s12274-021-3670-y

Section S1 TCAD simulation of the MoS_2 device with/without the capacitive MIS field-effect

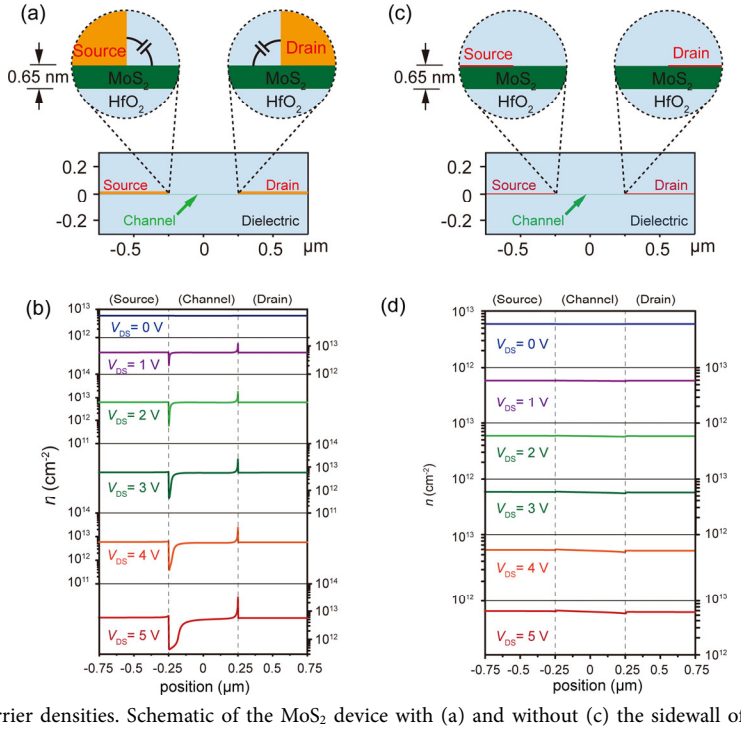

Figure S1 MoS_2 devices and carrier densities. Schematic of the MoS_2 device with (a) and without (c) the sidewall of the metallic electrode. Electron density distribution of the MoS_2 channel with (b) and without (d) the capacitive MIS field-effect.

Section S2 The field-effect for devices with various metal electrode thickness and channel thickness (layer number)

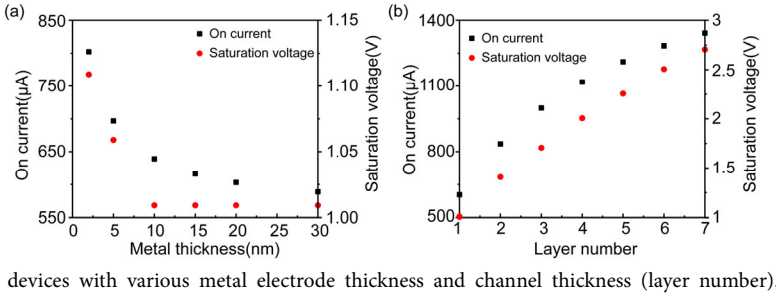

Figure S2 The field-effect for devices with various metal electrode thickness and channel thickness (layer number). (a) The elationship between on-current/saturation voltage (Min(d(dI_{DS}/dV_{Ds})/dV_{Ds})) and metal thickness. (b) The relationship between on-current/saturation voltage and the number of MoS_2 layers.

Address correspondence to Yao Guo, yaoguo@bit.edu.cn; Yang Chai, ychai@polyu.edu.hk

Section S3 Capacitive MIS field-effect to Schottky electrical contacts

The manuscript has discussed the principle of the capacitive MIS field-effect at Ohmic electrical contacts. A similar analysis applies to the Schottky contacts, too. In this case, we carry the same simulation and change the Ohmic contacts to the Schottky contacts with the barrier height of 300 meV. Fig. S3(a) shows the I-V curves without the capacitive MIS field-effect. The I-V curves are nonlinear with increased differential conductance. This nonlinearity is due to the increased tunneling current, which includes the direct field emission and the thermal-field emission. The large V_{DS} decrease the barrier width and increases the tunneling probability significantly. For the Schottky contacts with the capacitive MIS field-effect, as shown in Fig. S3(b), the I-V curves are nonlinear with current saturation. The capacitive MIS field-effect at the Source raises the conduction band energy, increases the barrier width, and therefore reduces the tunneling probability. The band graphs of the two cases are shown in Fig. S3(c) (without the capacitive MIS field-effect) and Fig. S3(d) (with the capacitive MIS field-effect), and zoomed in Fig. S3(e). The barrier width for the direct tunneling increase from 0.2 Å to 2.7 Å due to the capacitive MIS field-effect. The carrier densities are shown in Fig. S3(f).

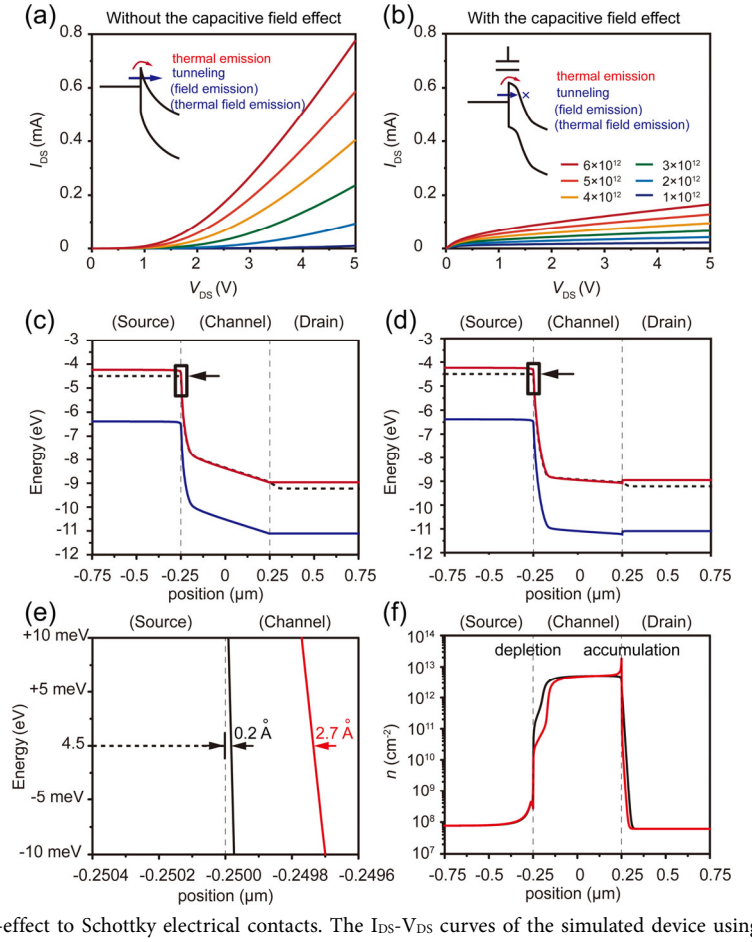

Figure S3 Capacitive MIS field-effect to Schottky electrical contacts. The I_{DS}-V_{DS} curves of the simulated device using the Schottky barrier of 0.3 eV without (a) and with (b) the capacitive MIS field-effect, the doping density of channel are shown in the legend of Fig. S3(b). Band graph of the device without (c) and with (d) the capacitive MIS field-effect, the solid red lines are the conduction bands, the solid blue lines are the valence bands, and the black dotted lines are the Fermi levels. V_{DS} = 5 V, the doping density of the channel is 6×10^{12} cm^{-2}. (e) Zoomed band graph at the Source end, the black/red lines are the conduction band without/with the capacitive MIS field-effect. The barrier width for the direct tunneling increase from 0.2 Å to 2.7 Å due to the capacitive MIS field-effect. (f) Electron density of the channel, the black/red lines are without/with the capacitive MIS field-effect, respectively.

Section S4 MoS_2 FET with Ni contacts

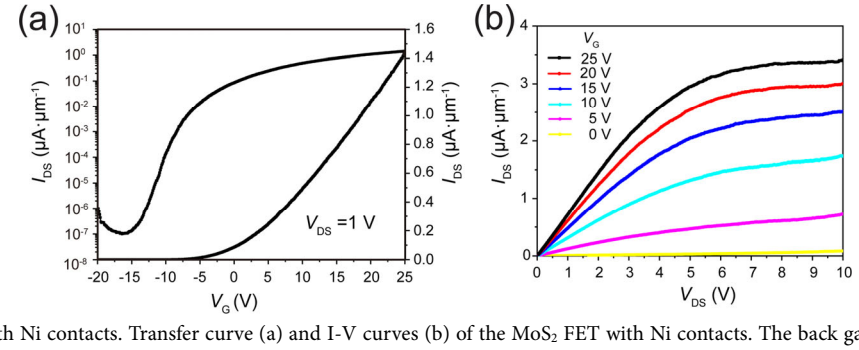

Figure S4 MoS_2 FET with Ni contacts. Transfer curve (a) and I-V curves (b) of the MoS_2 FET with Ni contacts. The back gate dielectric is 60 nm thick SiO_2, and the channel is CVD grown monolayer MoS_2. The channel length is 0.25 μm.

Section S5 TEM cross-section images of the electrical contacts to thin channels

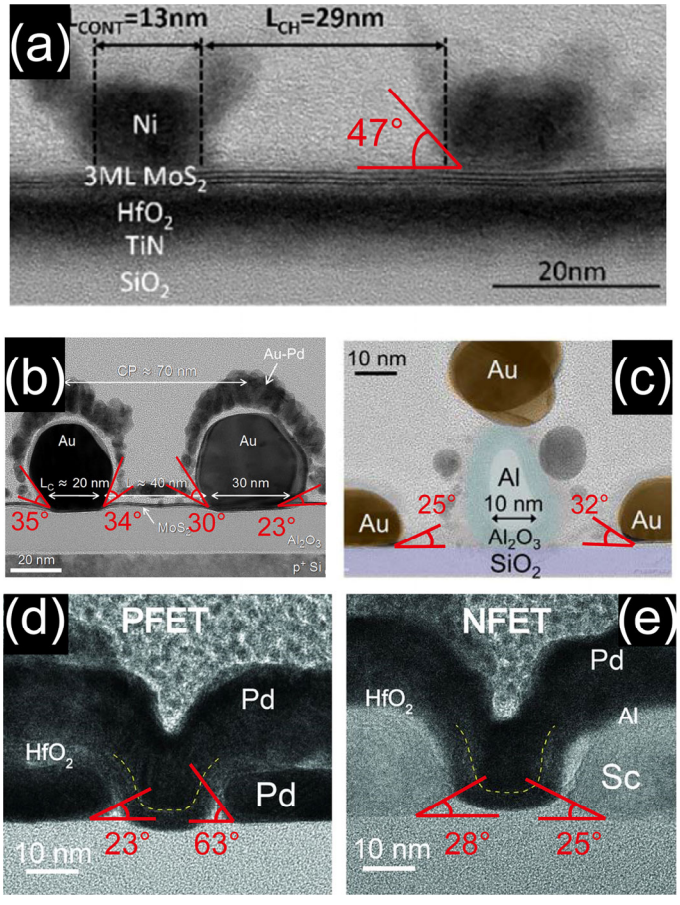

Figure S5 TEM images of the contacting angle of real devices. Cross-section of the Ni-MoS_2 contact (a) [1], the Au-MoS_2 contact (b) [2] and (c) [3], the Pd-carbon nanotube contact (d), and the Sc-carbon nanotube contact (e) [4]. Reproduced with permission from: ref. 1. Copyright Institute of Electrical and Electronics Engineers, 2019; ref. 2, Copyright American Chemical Society 2016; ref. 3, Copyright Institute of Electrical and Electronics Engineers, 2016; ref. 4, Copyright American Association for the Advancement of Science 2017.

Section S6 Enhanced capacitive MIS field-effect with the slanted sidewall

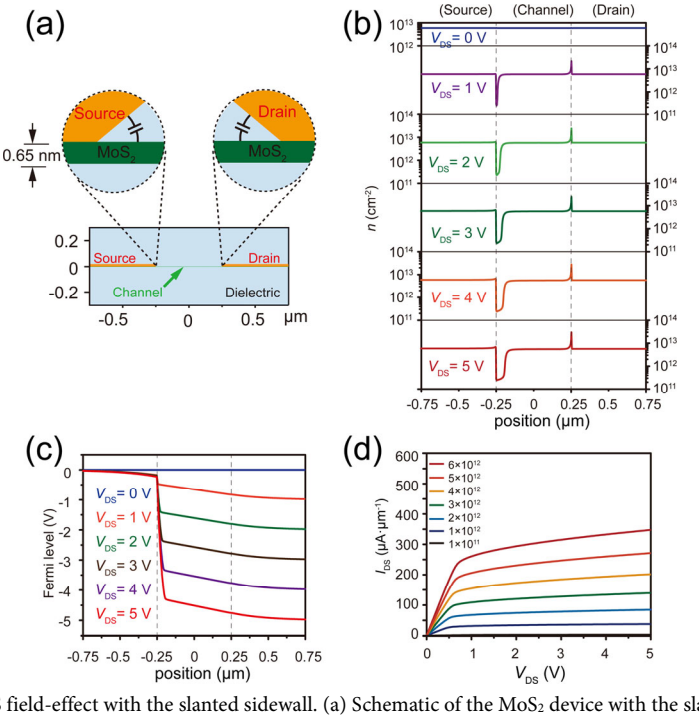

Figure S6 Enhanced capacitive MIS field-effect with the slanted sidewall. (a) Schematic of the MoS_2 device with the slanted sidewall. (b) Electron density of the MoS_2 channel. (c) Voltage potential along the MoS_2 channel. (d) Simulated I_{DS}-V_{DS} curves, the current saturation is significantly enhanced compared to the results in Fig. 1(f).

Section S7 Degeneration of MoS_2 transistors

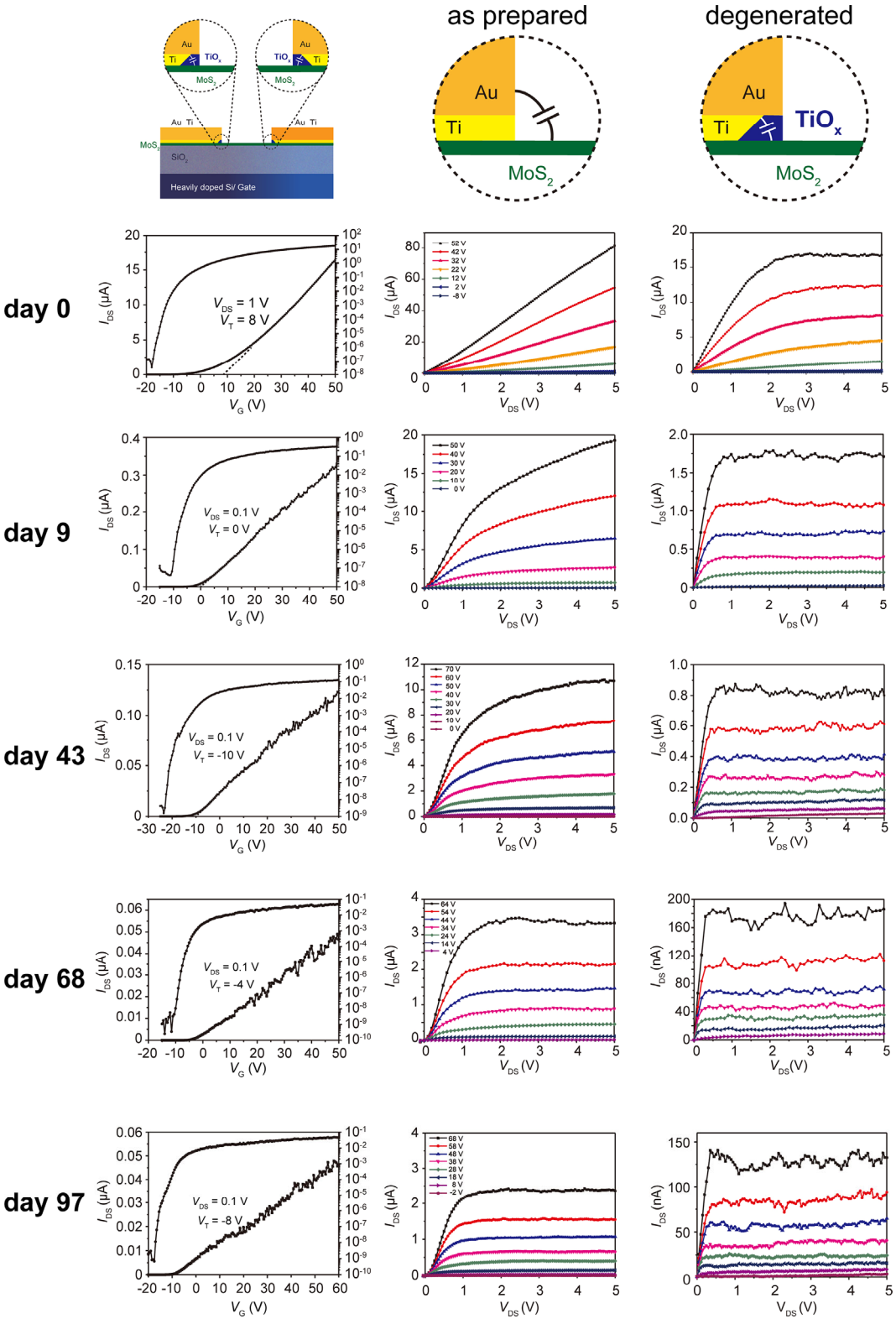

Figure S7 Degeneration of MoS_2 transistors. The degeneration of MoS_2 transistors is associated with the enhancement of the current saturation. As MoS_2 is super stable to the exposure of oxygen, the degeneration should result from the oxygen of Ti to TiO_x.

Section S8 Capacitive MIS field-effect of the electrical contacts to graphene

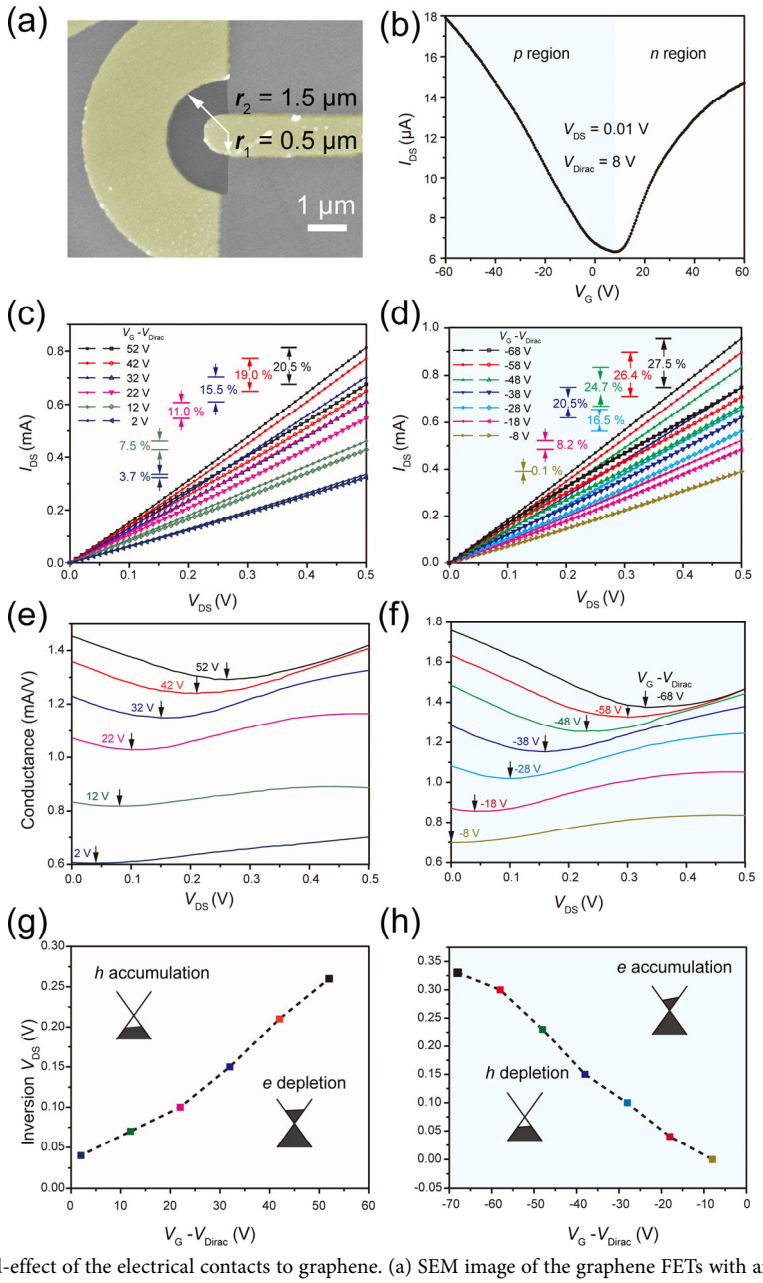

Figure S8 Capacitive MIS field-effect of the electrical contacts to graphene. (a) SEM image of the graphene FETs with arc channel. (b) Transfer curve of the graphene FET at V_{Dirac} = 8 V. (c) Compared I_{DS}-V_{DS} curves with the outer/inner electrode used as the Source/Drain (solid dot) and with the inner/outer electrode used as the Source/Drain (hollow dot). The channel is electron dominated (n region, V_G>V_{Dirac}). (d) Compared I_{DS}-V_{DS} curves with the outer/inner electrode used as the Source/Drain (solid dot) and with the inner/outer electrode used as the Source/Drain (hollow dot). The channel is hole dominated (p region, V_G<V_{Dirac}). (e) Differential conductance (smoothed) obtained from the n region I_{DS}-V_{DS} curve in Fig. 3(b) right, with the inner/outer electrode used as the Source/Drain. (f) Differential conductance (smoothed) obtained from the p region I_{DS}-V_{DS} curve in Fig. 3(e) right, with the inner/outer electrode used as the Source/Drain. (g-h) The inversion points extracted from (e) and (f), respectively.

Section S9 The fabrication process of the contacts with eliminated capacitive MIS field-effect

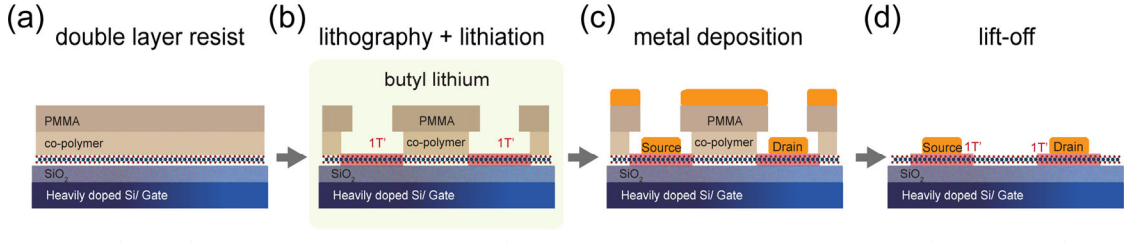

Figure S9 Schematic of device fabrication. (a) Double-layer resists of PMMA (up), and co-polymer (down) were used for EBL, which forms the extended space under the pattern. (b) The wafer was then immersed in butyl lithium for the 2H to 1T' transition of MoS_2. (c) The contacting electrodes are then deposited by the e-beam evaporation. (d) The resist and the redundant metal are removed by the lift-off process in acetone.

Section S10 10 nm gate length MoS_2 transistors with different contact configurations

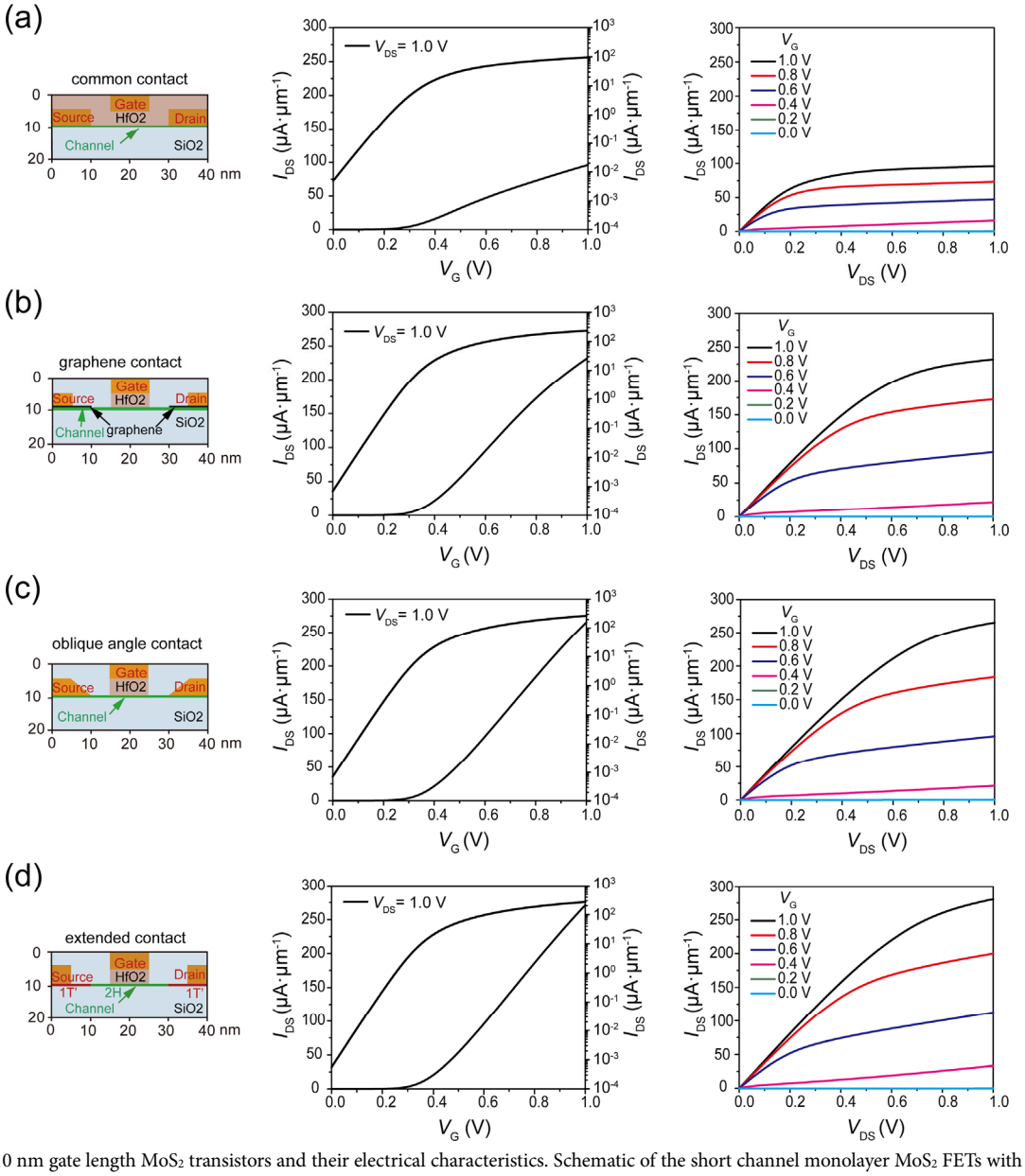

Figure S10 10 nm gate length MoS_2 transistors and their electrical characteristics. Schematic of the short channel monolayer MoS_2 FETs with the common contact configuration (a), the graphene contact configuration (b), the oblique angle contact configuration (c), and the extended contact configuration (d). The doping density of the channel is 6×10^{19} cm^{-2}. The threshold voltage is adjusted by the work function of the gate electrode (4.9 eV).

Section S11 Introducing nonlinearity to ANN circuits

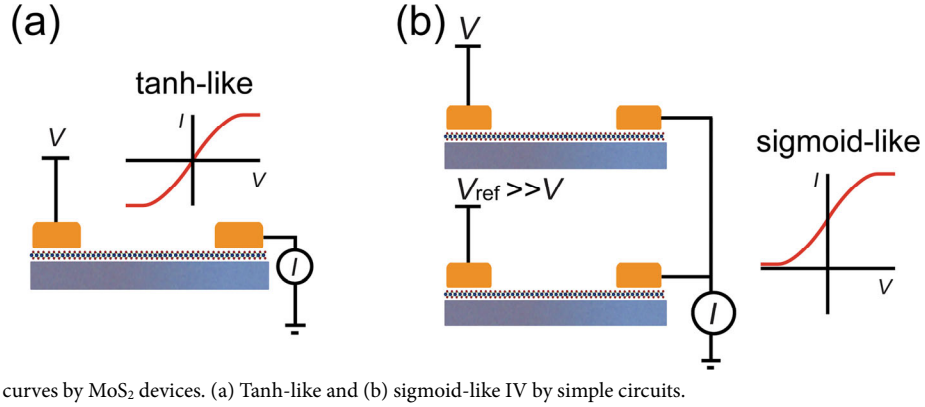

Figure S11 S-like IV curves by MoS_2 devices. (a) Tanh-like and (b) sigmoid-like IV by simple circuits.

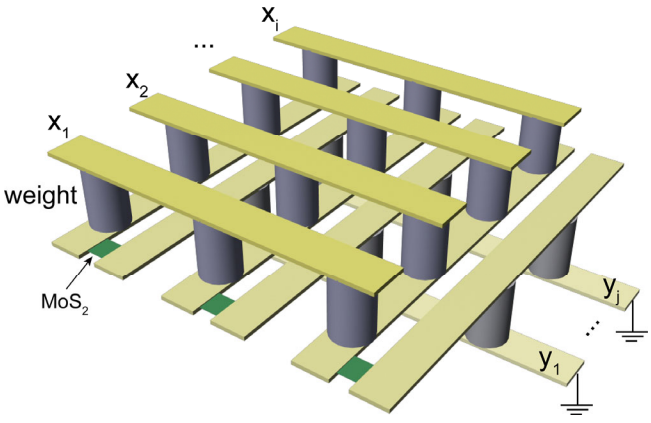

Figure S12 Compact structure of the hybrid ANN in-memory-computing circuit structure.

Reference

[1] Smets, Q.; Arutchelvan, G.; Jussot, J.; Verreck, D.; Asselberghs, I.; Mehta, A. N.; Gaur, A.; Lin, D.; Kazzi, S. E.; Groven, B. et al.; Ultra-scaled MOCVD MoS_2 MOSFETs with 42nm contact pitch and 250μA/μm drain current. In *Proceedings of the IEEE International Electron Devices Meeting (IEDM)*, San Francisco, CA, USA, **2019**, pp 23.22.21-23.22.24.

[2] English, C. D.; Shine, G.; Dorgan, V. E.; Saraswat, K. C., Pop, E.; Improved contacts to MoS_2 transistors by ultra-high vacuum metal deposition. *Nano Lett.* **2016**, 16, 3824-3830.

[3] English, C. D.; Smithe, K. K. H.; Xu, R. L., Pop, E.; Approaching ballistic transport in monolayer MoS_2 transistors with self-aligned 10 nm top gates. In *Proceedings of the IEEE International Electron Devices Meeting (IEDM)*, San Francisco, CA, USA, **2016**, pp 5.6.1-5.6.4.

[4] Qiu, C. G.; Zhang, Z. Y.; Xiao, M. M.; Yang, Y. J.; Zhong, D. L., Peng, L.-M.; Scaling carbon nanotube complementary transistors to 5-nm gate lengths. *Science* **2017**, 355, 271-276.